Electronic Supporting Information (ESI)

Physicochemical implications of alkoxide "mixing" in polyoxovanadium clusters for nonaqueous energy storage

*Lauren E. VanGelder,[a] Eric Schreiber,[a] and Ellen M. Matson[a]**

[a]Department of Chemistry, University of Rochester, Rochester, New York 14627

*Corresponding author email: matson@chem.rochester.edu

Supporting Information Table of Contents

Experimental Methods:

General Considerations. Manipulations that required the absence of water and oxygen were conducted in a UniLab MBraun inert atmosphere glovebox under a dinitrogen atmosphere. Glassware was oven dried for a minimum of 4 hours and cooled in an evacuated antechamber prior to use in the drybox. Anhydrous methanol, ethanol, propanol, butanol, pentanol, and hexanol were purchased from Sigma-Aldrich and stored over activated 4 Å molecular sieves purchased from Fisher Scientific. Anhydrous acetonitrile was dried and deoxygenated on a Glass Contour System (Pure Process Technology, LLC) and stored over activated 4 Å molecular sieves. $[^nBu_4N][BH_4]$ and V_2O_5 were purchased from Sigma-Aldrich and used as received. The supporting electrolyte $[^nBu_4N][PF_6]$ was purchased from Sigma-Aldrich, recrystallized three times using hot methanol, and stored under dynamic vacuum for a minimum of two days prior to use. $VO(O^tBu)_3$, $VO(OCH_3)_3$, **1-Methyl**, **1-Ethyl**, **1-Propyl**, and **1-Butyl** were prepared according to previous literature.[1, 2]

Mass spectrometry analyses were performed on an Advion expression^L Compact Mass Spectrometer equipped with an electrospray probe and an ion-trap mass analyzer. Direct injection analysis was employed in all cases with a sample solution in acetonitrile. ^1H NMR spectra were recorded at 500 on Bruker DPX-500 spectrometer locked on the signal of deuterated solvents. All chemical shifts were reported relative to the peak of residual ^1H signal in deuterated solvents. CD_3CN was purchased from Cambridge Isotope Laboratories, degassed by three freeze−pump−thaw cycles, and stored over activated 4 Å molecular sieves. Infrared (FT-IR, ATR) spectra of complexes were recorded on a Shimadzu IRAffinity-1 Fourier Transform Infrared Spectrophotometer and are reported in wavenumbers (cm^{-1}). Electronic absorption measurements were recorded at room temperature in anhydrous acetonitrile in a sealed 1 cm quartz cuvette with an Agilent Cary 60 UV-Vis spectrophotometer. Elemental analyses were performed on a PerkinElmer 2400 Series II Analyzer, at the CENTC Elemental Analysis Facility, University of Rochester.

Cyclic Voltammetry. Concentrations of active species (vanadium cluster) and $[NBu_4][PF_6]$ used were 1 mM and 100 mM, respectively. CV measurements were carried out using a Bio-Logic SP 150 potentiostat/galvanostat and the EC-Lab software suite. Glassy carbon discs (3 mm, CH Instruments, USA) were used as working electrodes. Working electrodes were polished using a micro cloth pad and 0.05 µM alumina powder. Potentials recorded during CV were measured relative to a nonaqueous Ag/Ag^+ reference electrode with 10 mM $AgNO_3$ and 100 mM $[^nBu_4N][PF_6]$ in acetonitrile (Bio-Logic). A platinum wire served as the counter electrode. All experiments were carried out at room temperature inside a nitrogen-filled glove box (MBraun, USA). All CV measurements were iR compensated at 85% with impedance taken at 100kHz using the ZIR tool included with the EC-Lab software.

Determining D_0 and k_0. Concentrations of active species (vanadium cluster) used were 1 mM with 0.1 M $[NBu_4][PF_6]$ supporting electrolyte. CV measurements were carried out inside a nitrogen filled glove box (MBraun, USA) using a Bio-Logic SP 150 potentiostat/galvanostat and the EC-Lab software suite. Cyclic voltammograms were recorded using a 3 mm diameter glassy carbon working electrode (CH Instruments, USA), a Pt wire auxiliary electrode (CH Instruments, USA), and a Ag/Ag^+ non-aqueous reference electrode with 0.01 M $AgNO_3$ in 0.1 M $[^nBu_4N][PF_6]$ in CH_3CN (Bio-Logic). Cyclic voltammograms were *iR* compensated at 85% with impedance taken at 100 kHz using the ZIR tool included in the EC-Lab software.

The diffusion coefficient associated with each neutral cluster was determined by using the slope of the peak current (i_p) of the oxidative wave (cathodic sweep) versus the square root of scan rate $\nu^{1/2}$. The Randles-Sevcik equation was used to estimate the diffusion coefficients from CV data. For a reversible redox couple, the peak current is given by the eq. S1;

$$i_p = 2.69 \times 10^5\, n^{3/2} A\, c\, D_0^{1/2}\, \nu^{1/2} \quad \text{Eq. S1}$$

In eq. S1, n is the number of electrons transferred; A is the electrode area (0.0707 cm^2 for the glassy carbon working electrode); c is the bulk concentration of the active species; D_0 is the diffusion coefficient of the active species; ν is the scan rate. For an irreversible redox couple, the peak current, is given by the eq. S2:

$$i_p = 2.99 \times 10^5\, n^{3/2}\, \alpha^{1/2}\, A\, c\, D_0^{1/2}\, \nu^{1/2} \qquad \text{Eq. S2}$$

where α is the charge transfer coefficient (α ~ 0.5).

For the redox couples that show quasi-reversible kinetics, relationships for both reversible and irreversible redox reaction are usually employed to determine the diffusion coefficients of such redox processes. Therefore, an average value of diffusion coefficient was approximated for a quasi-reversible redox couple using both equations S1 and S2.[3-5]

The Heterogeneous Electron-Transfer Rate Constants were calculated using the Nicholson method.[6] The potential difference (ΔEp) of oxidation and reduction peaks were obtained at different scan rates. The transfer parameter, ψ, was extracted from the working curve constructed by Nicholson using ΔEp values. The standard heterogeneous charge-transfer rate constant, k_0, for a given electron transfer process was determined using the following equation:

$$\psi = \frac{k_0}{(\frac{\pi n F D v}{RT})^{1/2}} \qquad \text{Eq. 3}$$

where n is the number of electrons transferred, F is the Faraday constant, D is the diffusion coefficient, v is the scan rate, R is the ideal gas constant and T is the temperature.[6, 7]

Parameters for chronoamperometry/bulk electrolysis experiments. Bulk electrolysis experiments were performed in a H-cell with a glass frit separator (Porosity =10-16 µm, Pine Research, USA) using a Bio-Logic SP 150 potentiostat/galvanostat. An active species concentration of 1 mM was used. Working electrode compartment contained 15 mL of the active species with 100 mM $[NBu_4][PF_6]$ in CH_3CN and counter electrode compartment had 15 mL of 100 mM $[^nBu_4N][PF_6]$ in CH_3CN. A Pt mesh working electrode and a Pt wire counter electrode were used. Bulk electrolysis experiments were carried out using the chronoamperometry techniques available in EC lab software suite at constant potentials, selected from CV.

Parameters for charge discharge experiments. Charge-discharge testing was carried out inside a nitrogen filled glove box (MBraun, USA) using a glass H-cell separated by a microporous glass frit (P5, 1.6 µm, Adams and Chittenden, USA). Each compartment contained stirring solutions (5 mL), with 1 mM active species and 100 mM $[^nBu_4N][PF_6]$ in acetonitrile. Two graphite felt electrodes (1 × 1 × 0.5 cm, Fuel Cell Store, USA) were attached to Pt wire current collectors and submerged in the posolyte and negolyte chambers (~0.5 cm), where they were allowed to soak for 12 hours prior to the start of the experiment. Experiments were conducted using a Bio-Logic SP 150 potentiostat/galvanostat with galvanostatic charging and discharging conditions at 0.1 mA.

Synthetic Preparations:

Synthesis of homoleptic POV-alkoxides, $V_6O_7(OR)_{12}$ (R = C_5H_{11}, C_6H_{13}).

In the glovebox, $VO(O^tBu)_3$ (0.250 g, 0.9 mmol), $[^nBu_4N][BH_4]$ (0.075 g, 0.3 mmol), and the respective alcohol R-OH (8 mL, R = C_5H_{11} or C_6H_{13}) were charge in a 25 mL Teflon-lined autoclave (PARR). The steel reaction vessel was sealed, and the mixture heated to 125 °C for 24 h. After the allotted time period, the autoclave was cooled to room temperature, and the subsequent workup completed in ambient atmosphere. The resulting green solution was dried under reduced pressure to obtain a dark green oil, identified as the respective anionic clusters $[^nBu_4N][V_6O_7(OR)_{12}]$. Oxidation to form the neutral cluster was accomplished by adding a solution of I_2 (0.050 g, 0.197 mmol) in acetonitrile (20 mL) to the crude solid with stirring overnight. The acetonitrile was removed under reduced pressure and the products **$[V_6O_7(OC_5H_{11})_{12}]$** or **$[V_6O_7(OC_5H_{13})_{12}]$** extracted with hexanes for use.

$[V_6O_7(OC_5H_{11})_{12}]$ (1-Pentyl). Appearance: dark green oil at room temperature. Yield: 0.186 g, 0.13 mmol, 87 %. ^{1}H NMR (500 MHz, CD_3CN): δ = 21.64 (br). UV−Vis (CH_3CN) [ε (M^{-1} cm^{-1})]: 392 nm (2.58 x 10^3), 1000 nm (3.91 x 10^2). ESI-MS (+): *m/z* 1463.

$[V_6O_7(OC_6H_{13})_{12}]$ (1-Hexyl). Appearance: dark green oil at room temperature. Yield: 0.166 g, 0.10 mmol, 70 %. ^{1}H NMR (500 MHz, CD_3CN): δ = 21.74 (br). UV−Vis (CH_3CN) [ε (M^{-1} cm^{-1})]: 392 nm (1.01 x 10^3), 1000 nm (1.47 x 10^2). ESI-MS (+): *m/z* 1632.

Synthesis of heteroleptic "mixed" POV-alkoxides, $V_6O_7(OR)_{12-x}(OCH_3)_x$ ($R = C_2H_5, C_3H_7, C_4H_9, C_5H_{11}, C_6H_{13}$).

In the glovebox, $VO(OCH_3)_3$ (0.300 g, 1.9 mmol), $[{}^{n}Bu_4N][BH_4]$ (0.080 g, 0.3 mmol), and the respective alcohol R-OH (8 mL, $R = C_2H_5$, C_3H_7, C_4H_9, C_5H_{11} or C_6H_{13}) were charge in a 25 mL Teflon-lined autoclave (PARR). The reaction vessel was sealed, and the mixture heated to 125 °C for 24 h. After the allotted time period, the autoclave was cooled to room temperature, and the subsequent workup completed in ambient atmosphere. The resulting green solution was dried under reduced pressure to obtain the crude products, identified as the respective anionic clusters $[{}^{n}Bu_4N][V_6O_7(OR)_{12-x}(OCH_3)_x]$. Oxidation to form the neutral cluster was accomplished by adding a solution of I_2 (0.050 g, 0.197 mmol) in acetonitrile (20 mL) to the crude solid with stirring overnight. The acetonitrile was removed under reduced pressure and the products extracted with hexanes for use. Yields for mixtures calculated using average product mass from ESI-MS data.

$[V_6O_7(OC_2H_5)_{12-x}(OCH_3)_x]$ (2-Ethyl). Appearance: Dark green solid at room temperature. Yield: 0.069 g, 0.08 mmol, 24 %. ^{1}H NMR (500 MHz, CD_3CN): $\delta = 21.54$ (br). UV−Vis (CH_3CN) [ε (M^{-1} cm^{-1})]: 386 nm (2.23 x 10^3), 1000 nm (5.16 x 10^2). ESI-MS (+): *m/z* 944 ($[V_6O_7(OC_2H_5)_{11}(OCH_3)_1]$), 930 ($[V_6O_7(OC_2H_5)_{10}(OCH_3)_2]$), 916 ($[V_6O_7(OC_2H_5)_9(OCH_3)_3]$), 902 ($[V_6O_7(OC_2H_5)_8(OCH_3)_4]$), 888 ($[V_6O_7(OC_2H_5)_7(OCH_3)_5]$), 874 ($[V_6O_7(OC_2H_5)_6(OCH_3)_6]$).

$[V_6O_7(OC_3H_7)_{12-x}(OCH_3)_x]$ (2-Propyl). Appearance: Sticky green solid at room temperature. Yield: 0.149 g, 0.15 mmol, 48 %. ^{1}H NMR (500 MHz, CD_3CN): $\delta = 21.58$ (br). UV−Vis (CH_3CN) [ε (M^{-1} cm^{-1})]: 388 nm (7.19 x 10^3), 1000 nm (1.05 x 10^3). ESI-MS (+): *m/z* 1099 ($[V_6O_7(OC_3H_7)_{11}(OCH_3)_1]$), 1071 ($[V_6O_7(OC_3H_7)_{10}(OCH_3)_2]$), 1043 ($[V_6O_7(OC_3H_7)_9(OCH_3)_3]$), 1015 ($[V_6O_7(OC_3H_7)_8(OCH_3)_4]$), 1015 ($[V_6O_7(OC_3H_7)_7(OCH_3)_5]$), 959 ($[V_6O_7(OC_3H_7)_6(OCH_3)_6]$).

$[V_6O_7(OC_4H_9)_{12-x}(OCH_3)_x]$ (2-Butyl). Appearance: Dark green oil at room temperature. Yield: 0.153 g, 0.15 mmol, 47 %. ^{1}H NMR (500 MHz, CD_3CN): $\delta = 21.69$ (br). UV−Vis (CH_3CN) [ε (M^{-1} cm^{-1})]: 388 nm (7.23 x 10^3), 1000 nm (9.64 x 10^2). ESI-MS (+): *m/z* 1253 ($[V_6O_7(OC_4H_9)_{11}(OCH_3)_1]$), 1211 ($[V_6O_7(OC_4H_9)_{10}(OCH_3)_2]$), 1169 ($[V_6O_7(OC_4H_9)_9(OCH_3)_3]$), 1127 ($[V_6O_7(OC_4H_9)_8(OCH_3)_4]$), 1085 ($[V_6O_7(OC_4H_9)_7(OCH_3)_5]$), 1043 ($[V_6O_7(OC_4H_9)_6(OCH_3)_6]$), 1001 ($[V_6O_7(OC_4H_9)_5(OCH_3)_7]$).

$[V_6O_7(OC_5H_{11})_{12-x}(OCH_3)_x]$ (2-Pentyl) . Appearance: Dark green oil at room temperature. Yield: 0.328 g, 0.31 mmol, 98 %. ^{1}H NMR (500 MHz, CD_3CN): $\delta = 21.76$ (br). UV−Vis (CH_3CN) [ε (M^{-1} cm^{-1})]: 384 nm (3.88 x 10^3), 1000 nm (5.32 x 10^2). ESI-MS (+): *m/z* 1295 ($[V_6O_7(OC_5H_{11})_9(OCH_3)_3]$), 1239 ($[V_6O_7(OC_5H_{11})_8(OCH_3)_4]$), 1183 ($[V_6O_7(OC_5H_{11})_7(OCH_3)_5]$), 1127 ($[V_6O_7(OC_5H_{11})_6(OCH_3)_6]$), 1071 ($[V_6O_7(OC_5H_{11})_5(OCH_3)_7]$), 1029 ($[V_6O_7(OC_5H_{11})_4(OCH_3)_8]$).

$[V_6O_7(OC_6H_{13})_{12-x}(OCH_3)_x]$ (2-Hexyl). Appearance: Dark green oil at room temperature. Yield: 0.485 g, 0.30 mmol, 95 %. ^{1}H NMR (500 MHz, CD_3CN): $\delta = 21.91$ (br). UV−Vis (CH_3CN) [ε (M^{-1} cm^{-1})]: 384 nm (2.20 x 10^3), 1000 nm (3.07 x 10^2). ESI-MS (+): *m/z* 1421 ($[V_6O_7(OC_6H_{13})_9(OCH_3)_3]$), 1351 ($[V_6O_7(OC_6H_{13})_8(OCH_3)_4]$), 1281 ($[V_6O_7(OC_6H_{13})_7(OCH_3)_5]$), 1211 ($[V_6O_7(OC_6H_{13})_6(OCH_3)_6]$), 1141 ($[V_6O_7(OC_6H_{13})_5(OCH_3)_7]$), 1071 ($[V_6O_7(OC_6H_{13})_4(OCH_3)_8]$), 1001 ($[V_6O_7(OC_6H_{13})_3(OCH_3)_9]$).

Figure S1. Mass spec of homoleptic clusters **1-pentyl** and **1-hexyl**. Predicted spectra obtained using the Advion Expression^L software are shown above, with raw spectra below.

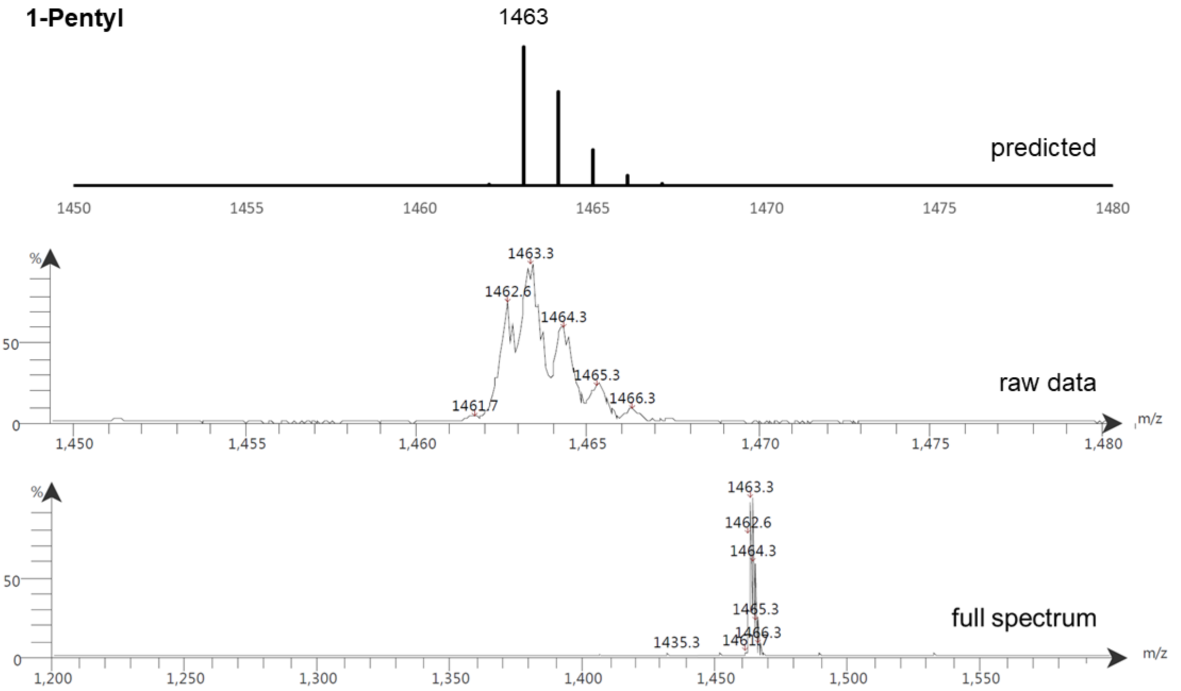

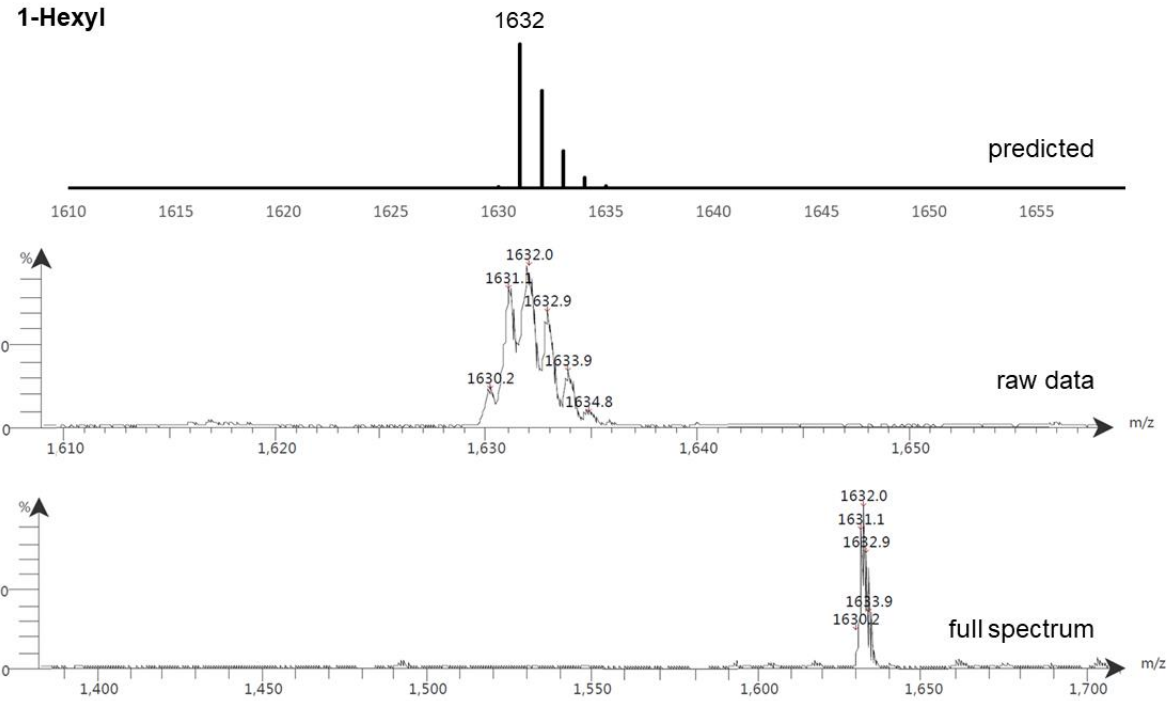

Figure S2. ^{1}H NMR of **1-Pentyl** and **1-Hexyl** in CD_3CN

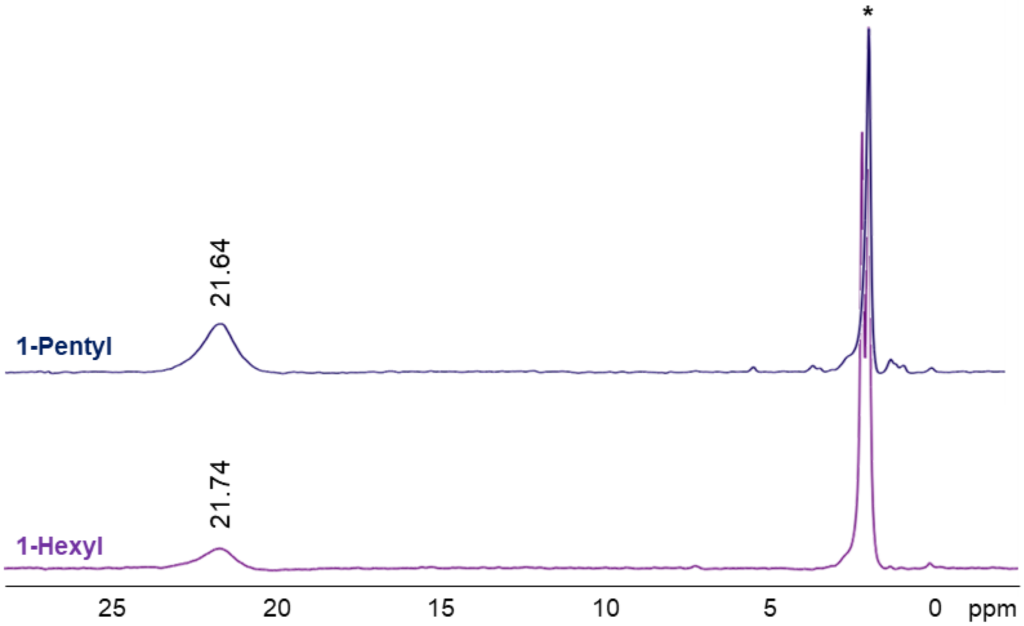

Figure S3. IR of **1-Pentyl** and **1-Hexyl**

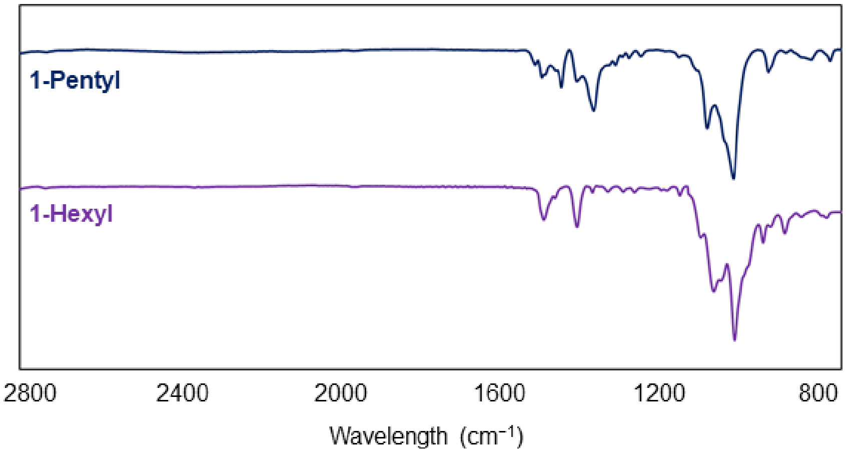

Figure S4. Beer's Law plots and solubility calculations for **1-Pentyl** in MeCN with 0.1 M [^{n}Bu$_4$N][PF$_6$]. Absorption spectra blanked with 0.1 M [^{n}Bu$_4$N][PF$_6$].

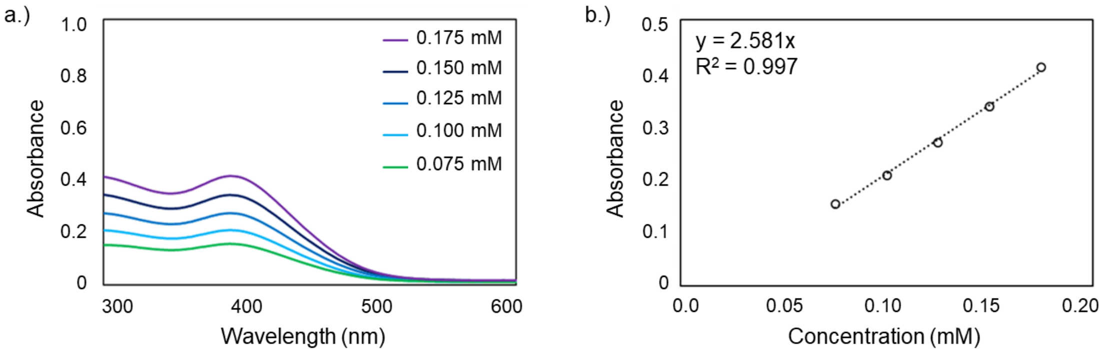

Trial	Absorbance (392 nm)	Dilute Concentration (mM)	Dilution	Saturated Concentration (M)
1	0.5043	0.195	20 µL to 10 mL	0.097
2	0.5730	0.222	20 µL to 10 mL	0.111
3	0.4800	0.186	20 µL to 10 mL	0.093

Average Concentration = 0.101 ± 0.009 M

Figure S5. Beer's Law plots and solubility calculations for **1-Hexyl** in MeCN with 0.1 M [^{n}Bu$_4$N][PF$_6$]. Absorption spectra blanked with 0.1 M [^{n}Bu$_4$N][PF$_6$].

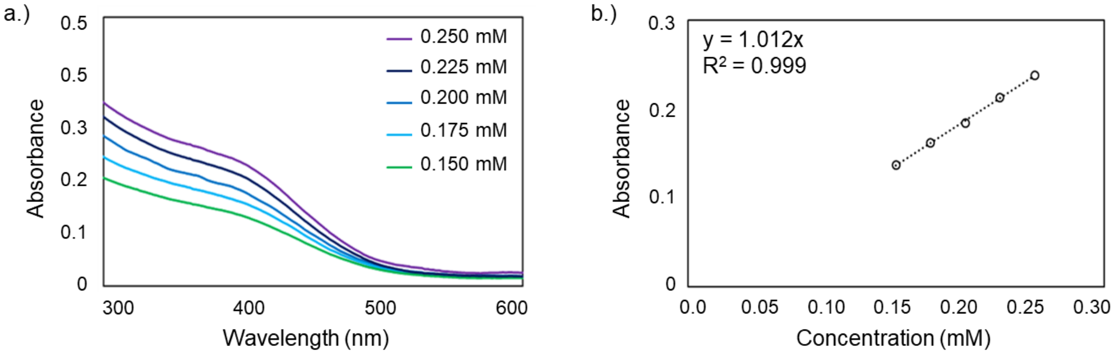

Trial	Absorbance (392 nm)	Dilute Concentration (mM)	Dilution	Saturated Concentration (M)
1	0.1746	0.173	25 µL to 10 mL	0.069
2	0.1290	0.128	25 µL to 10 mL	0.051
3	0.1113	0.110	25 µL to 10 mL	0.044

Average Concentration = 0.055 ± 0.013 M

Figure S6. CV **1-Hexyl** (1 mM) recorded at 100 mV/s in MeCN with 0.1 M [^{n}Bu$_4$N][PF$_6$].

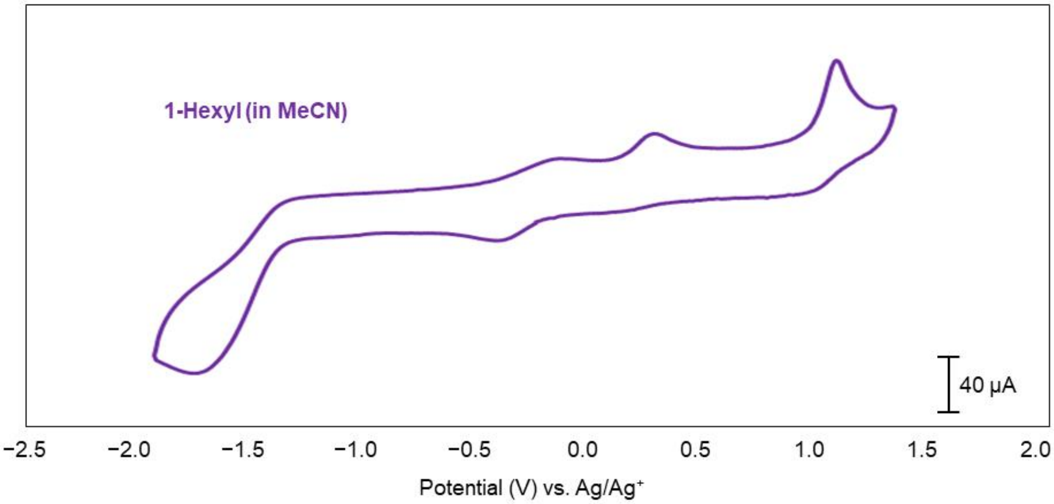

Figure S7. CV of **1-Hexyl** (1 mM) recorded at 100 mV/s in DCM with 0.1 M [^{n}Bu$_4$N][PF$_6$].

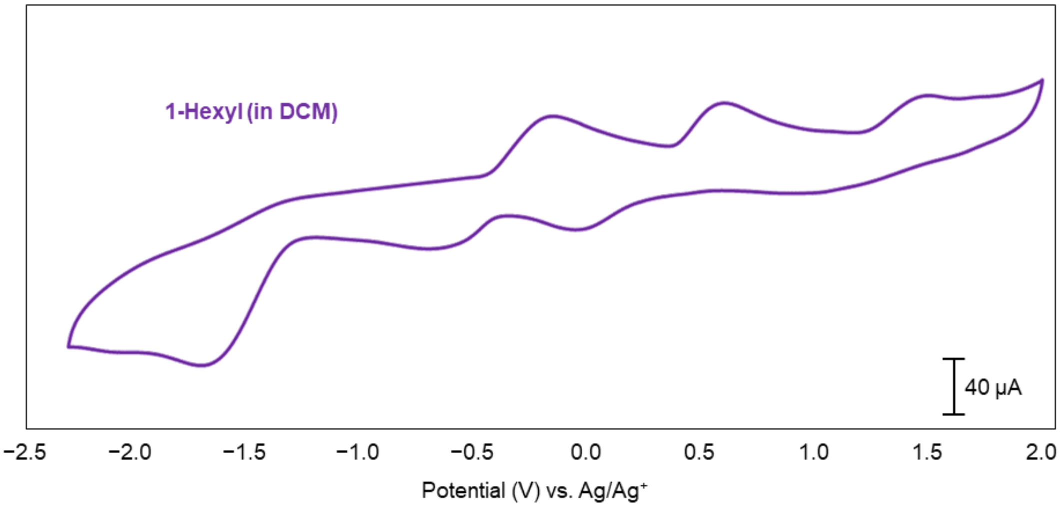

Figure S8. ESI-MS of **1-Butyl**. *m/z* = 1294 corresponds to the homoleptic compound $[V_6O_7(OC_4H_9)_{12}]$, while *m/z* = 1252 corresponds to the “impure” complex $[V_6O_7(OC_4H_9)_{11}(OCH_3)_1]$.

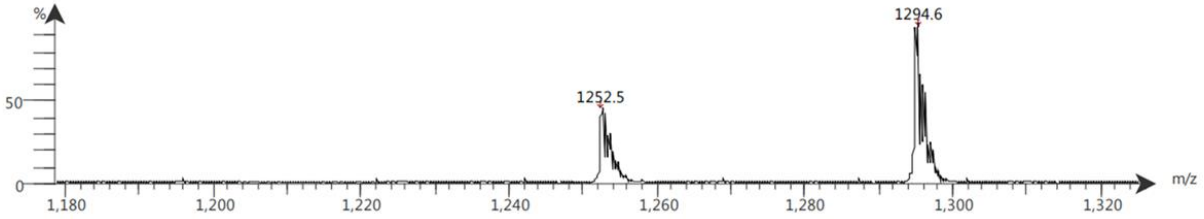

Figure S9. Electrospray ionization mass spectra of heteroleptic “mixed” clusters (a) **2-Ethyl** and (b) **2-Propyl**. Spectra for three separate trials are displayed, showing the consistency in product distribution.

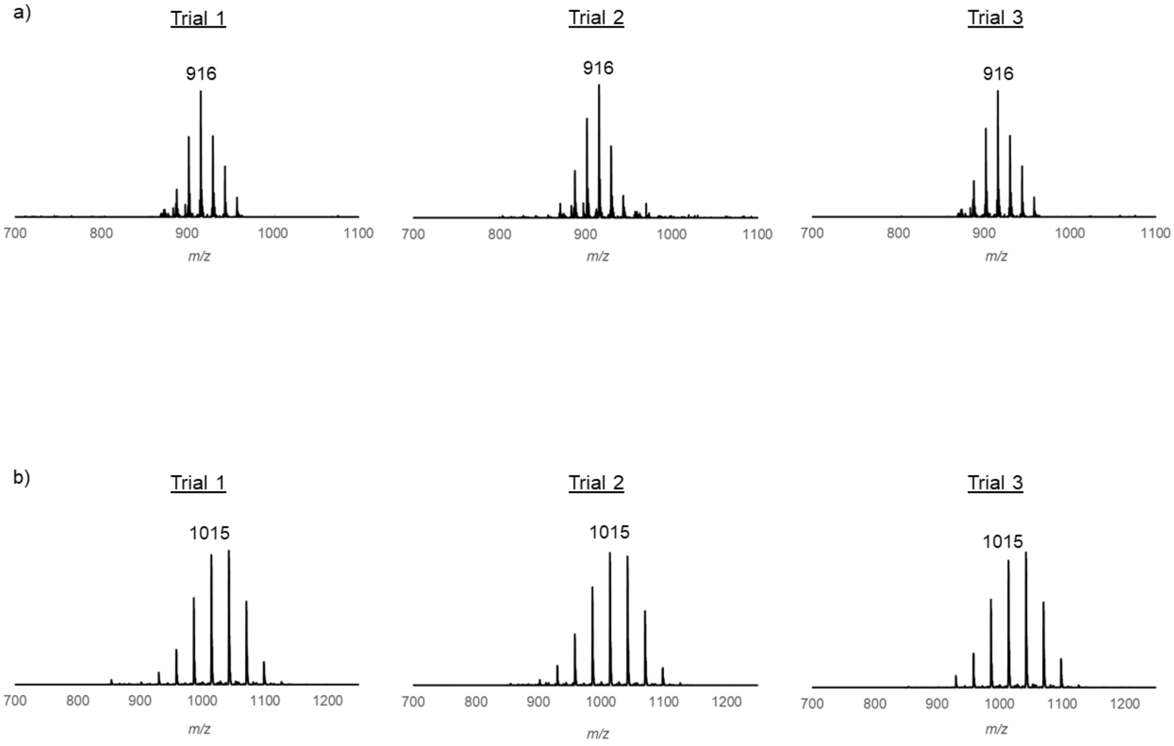

Figure S9 (continued). Electrospray ionization mass spectra of heteroleptic “mixed” clusters (c) **2-Butyl** (d) **2-Pentyl** and (e) **2-Hexyl** . Spectra for three separate trials are displayed, showing the consistency in product distribution.

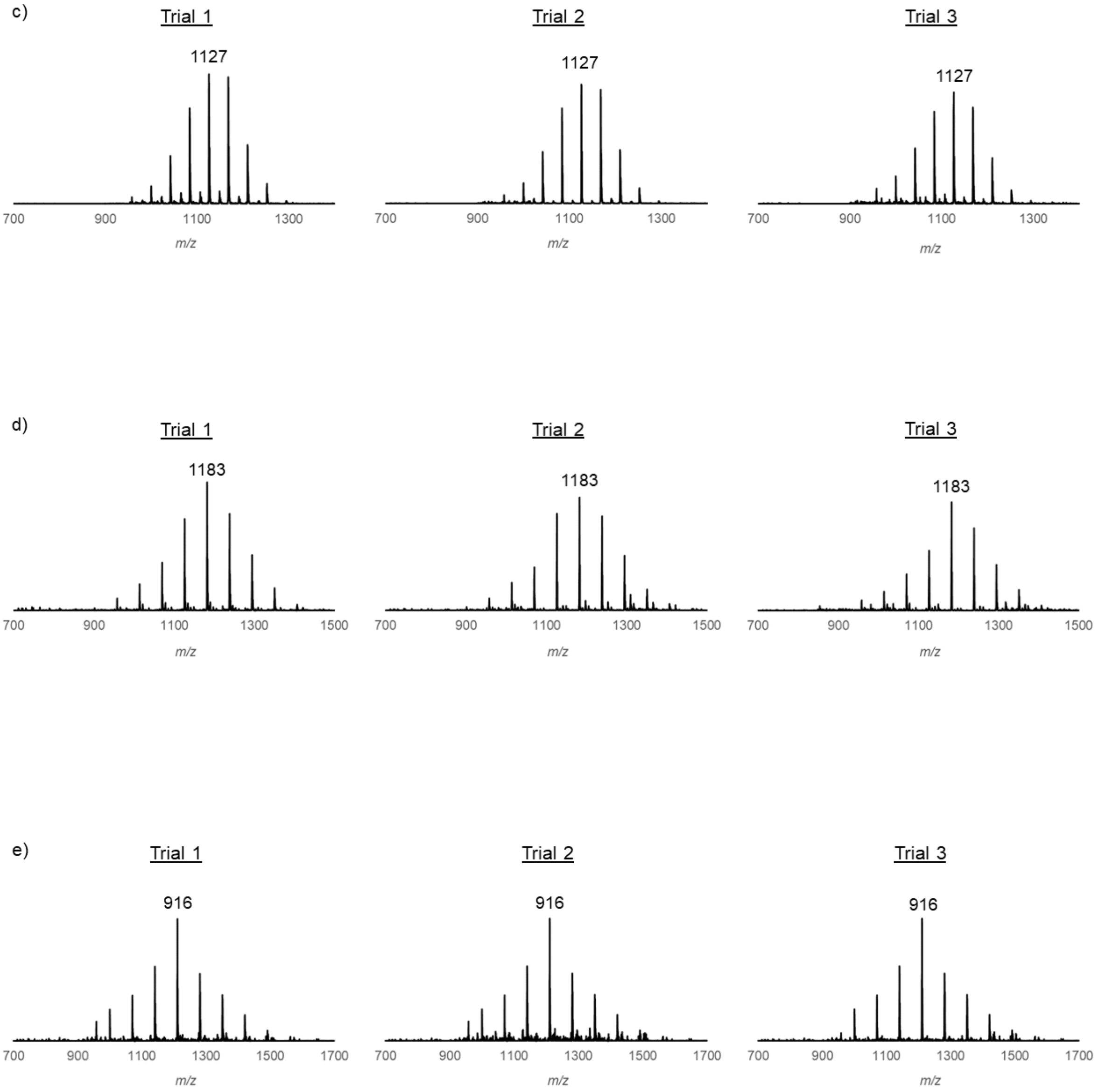

Figure S10. Electrospray ionization mass spectra of all heteroleptic “mixed” clusters, with chemical formula $[V_6O_7(OR)_{12-x}(OCH_3)_x]$. X values displayed over corresponding *m/z* values.

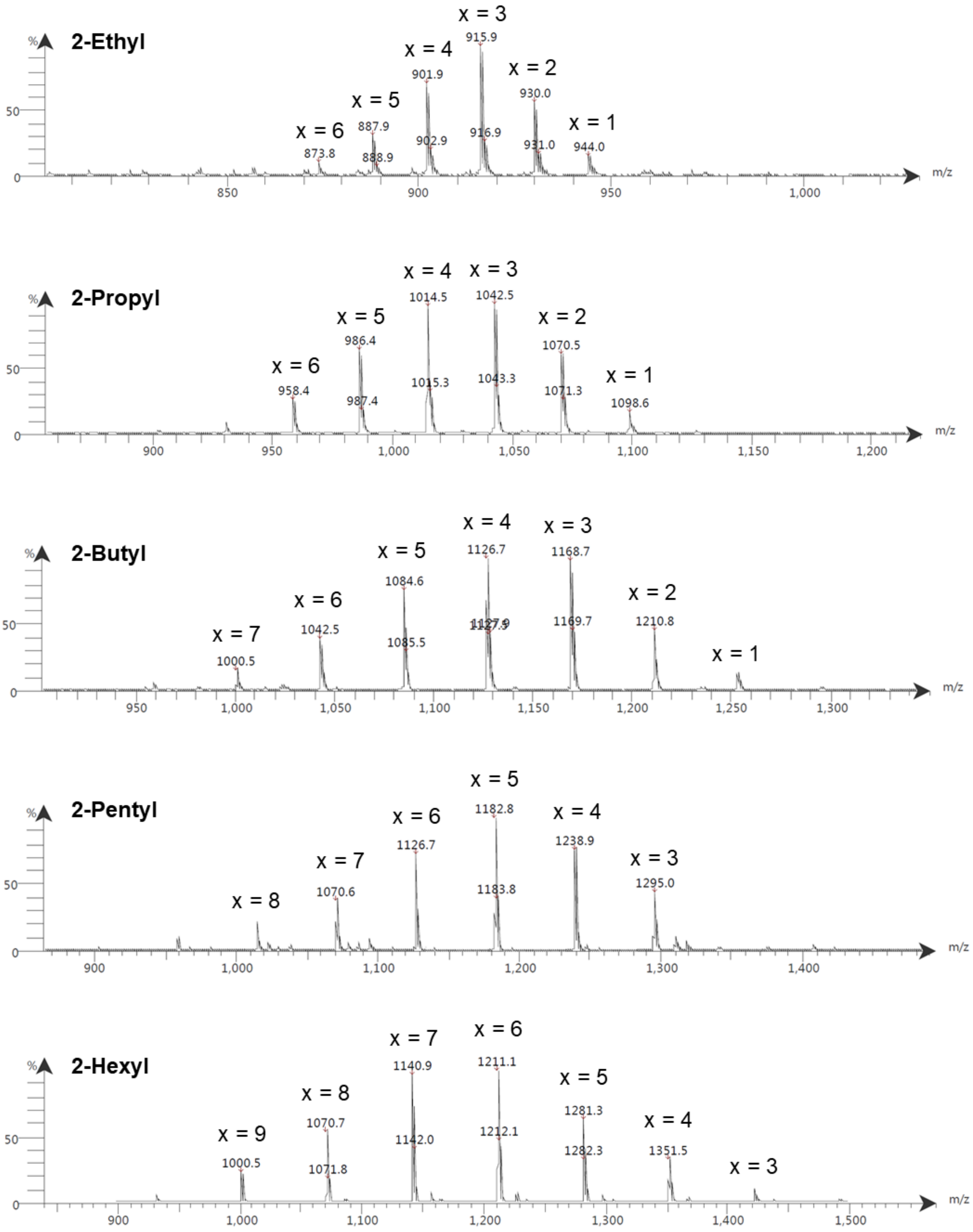

Figure S11. Average value of "x" in $V_6O_7(OR)_{12-x}(OCH_3)_x$ measured in the mass spectra of **2-Ethyl**, **2-Propyl**, **2-Butyl**, **2-Pentyl**, and **2-Hexyl**. As the carbon chain length (R) increases, the proportion of bridging methyl groups (x) to longer chain alkyl bridging R groups increases.

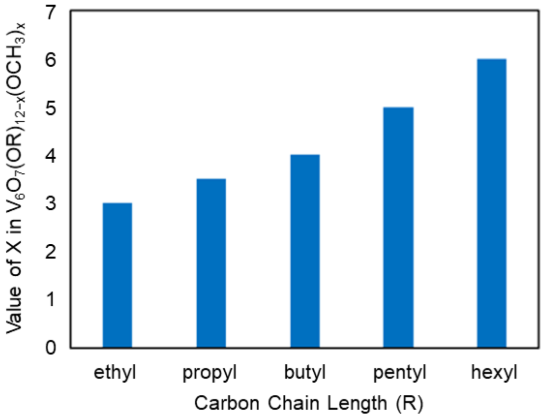

Figure S12. ^1H NMR of all heteroleptic "mixed" clusters in CD_3CN

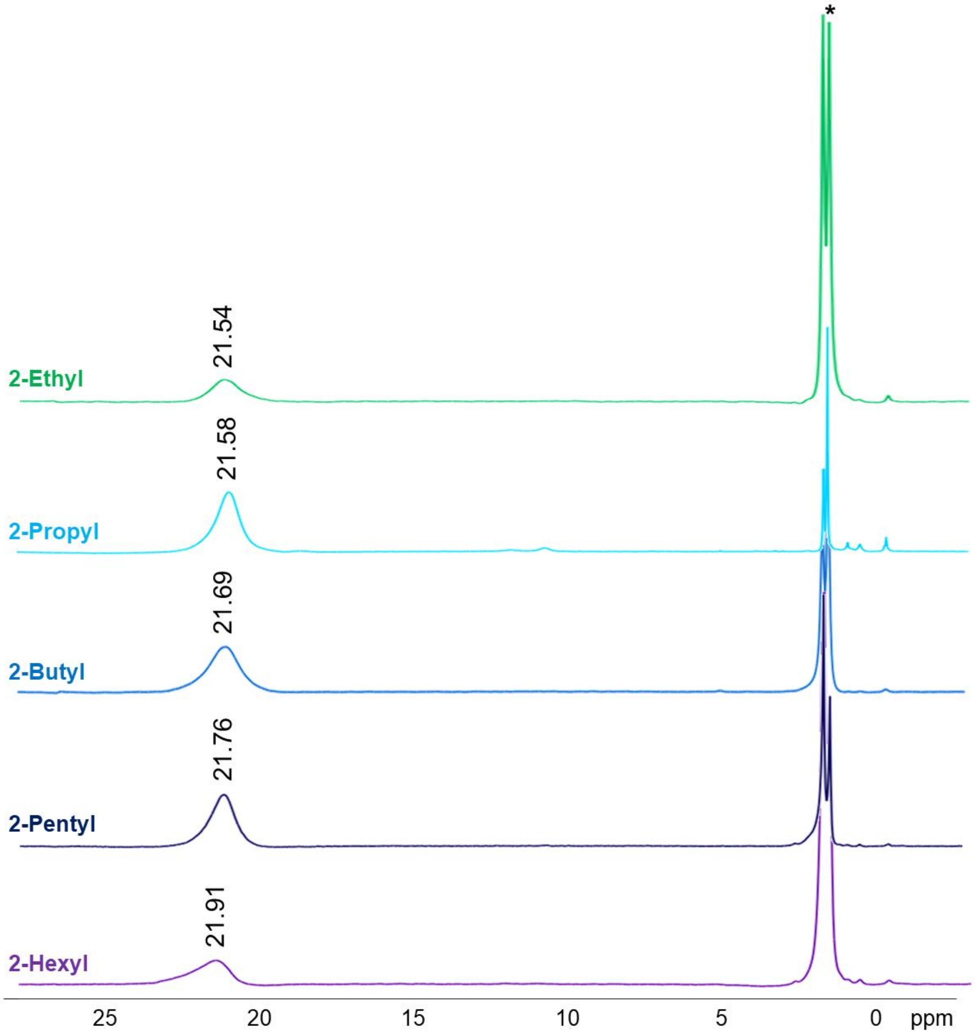

Figure S13. IR spectra of all heteroleptic “mixed” POV-alkoxides

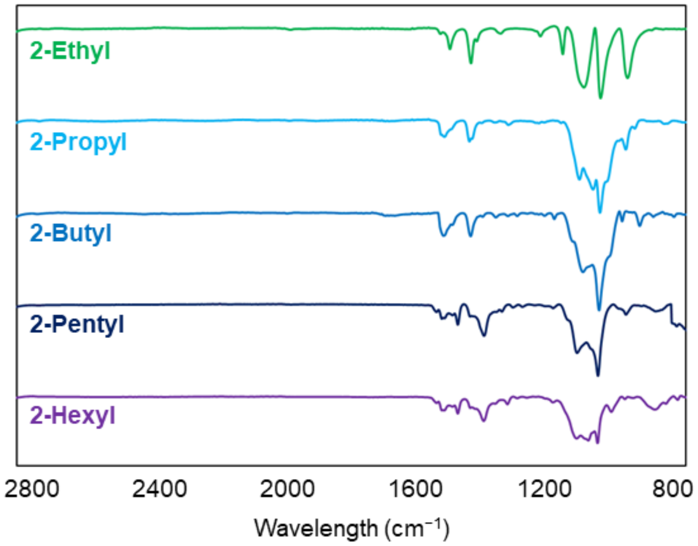

Figure S14. CV of **1-hexyl** and **2-hexyl** in MeCN

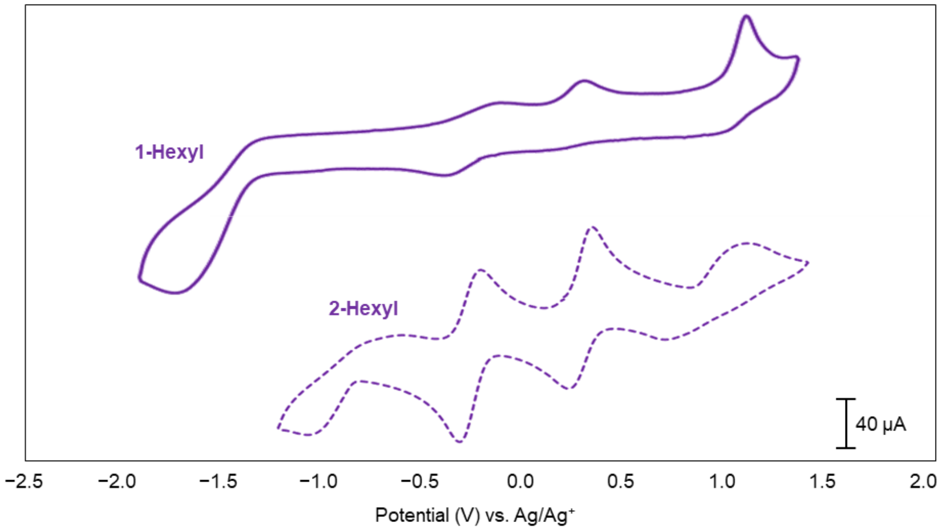

Complex	V^{IV}_6 / $V^{V}_1V^{IV}_5$	$V^{V}_1V^{IV}_5$ / $V^{V}_2V^{IV}_4$	$V^{V}_2V^{IV}_4$ / $V^{V}_3V^{IV}_3$	$V^{V}_3V^{IV}_3$ / $V^{V}_4V^{IV}_2$
1-Hexyl	−1.50 (0.00)	−0.32 (0.37)	0.30 (3.13)	1.11 (27.7)
2-Hexyl	−0.79 (0.75)	−0.28 (0.91)	0.28 (1.08)	0.93 (1.30)

Standard potentials (measured *vs*. Ag/Ag$^+$) identified using cyclic voltammetry at 100 mV s^{-1} of 1 mM solutions of each complex with 0.1 M [^{n}Bu$_4$N][PF$_6$] supporting electrolyte in acetonitrile. Values in parentheses indicate ratios of the cathodic to anodic peak heights (i_c/i_a).

Figure S15. CV of **1-hexyl** and **2-hexyl** in DCM

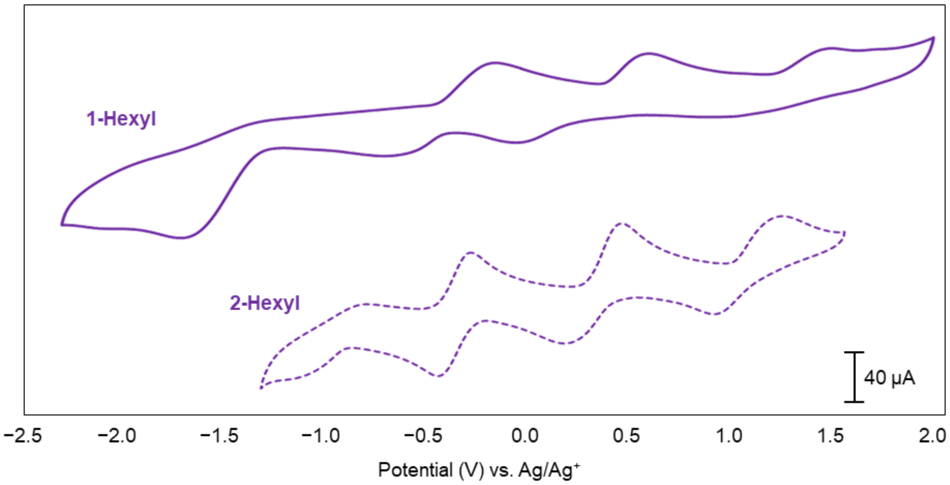

Complex	V^{IV}_6 / $V^{V}_1V^{IV}_5$	$V^{V}_1V^{IV}_5$ / $V^{V}_2V^{IV}_4$	$V^{V}_2V^{IV}_4$ / $V^{V}_3V^{IV}_3$	$V^{V}_3V^{IV}_3$ / $V^{V}_4V^{IV}_2$
1-Hexyl	−1.51 (0.04)	−0.42 (1.34)	0.27 (1.29)	1.25 (45.9)
2-Hexyl	−0.97 (0.73)	−0.37 (0.96)	0.32 (1.12)	1.08 (1.31)

Standard potentials (measured *vs*. Ag/Ag$^+$) identified using cyclic voltammetry at 100 mV s^{-1} of 1 mM solutions of each complex with 0.1 M [^{n}Bu$_4$N][PF$_6$] supporting electrolyte in DCM. Values in parentheses indicate ratios of the cathodic to anodic peak heights (i_c/i_a).

Figure S16. Beer's Law plots and solubility calculations for **2-Ethyl** in MeCN with 0.1 M [^{n}Bu$_4$N][PF$_6$]. Absorption spectra blanked with 0.1 M [^{n}Bu$_4$N][PF$_6$].

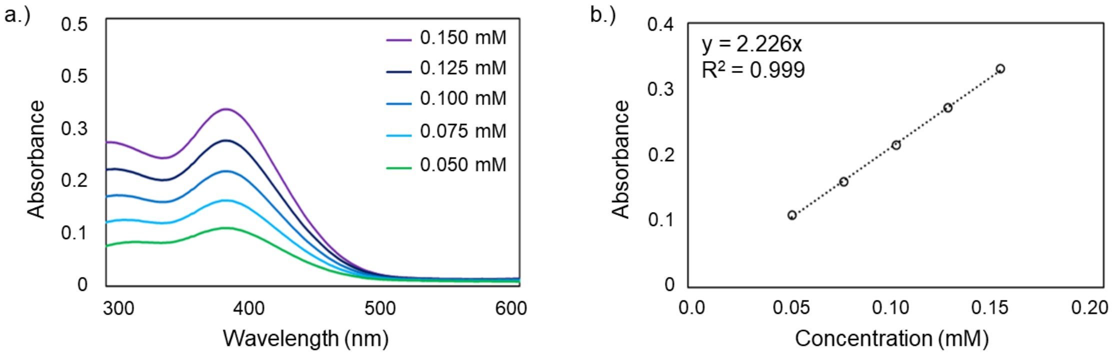

Trial	Absorbance (386 nm)	Dilute Concentration (mM)	Dilution	Saturated Concentration (M)
1	0.1291	0.0581	25 µL to 10 mL	0.058
2	0.1625	0.0729	25 µL to 10 mL	0.073
3	0.1803	0.0814	25 µL to 10 mL	0.081

Average Concentration = 0.071 ± 0.012 M

Figure S17. Beer's Law plots and solubility calculations for **2-Propyl** in MeCN with 0.1 M [^{n}Bu$_4$N][PF$_6$]. Absorption spectra blanked with 0.1 M [^{n}Bu$_4$N][PF$_6$].

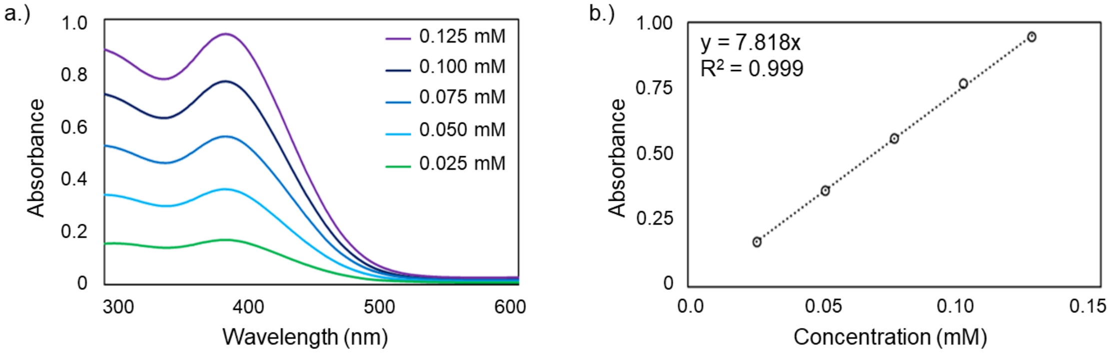

Trial	Absorbance (388 nm)	Dilute Concentration (mM)	Dilution	Saturated Concentration (M)
1	0.7186	0.0919	10 µL to 20 mL	0.184
2	0.6465	0.0827	10 µL to 20 mL	0.165
3	0.6772	0.0866	10 µL to 20 mL	0.173

Average Concentration = 0.174 ± 0.009 M

Figure S18. Beer's Law plots and solubility calculations for **2-Butyl** in MeCN with 0.1 M [^{n}Bu$_4$N][PF$_6$]. Absorption spectra blanked with 0.1 M [^{n}Bu$_4$N][PF$_6$].

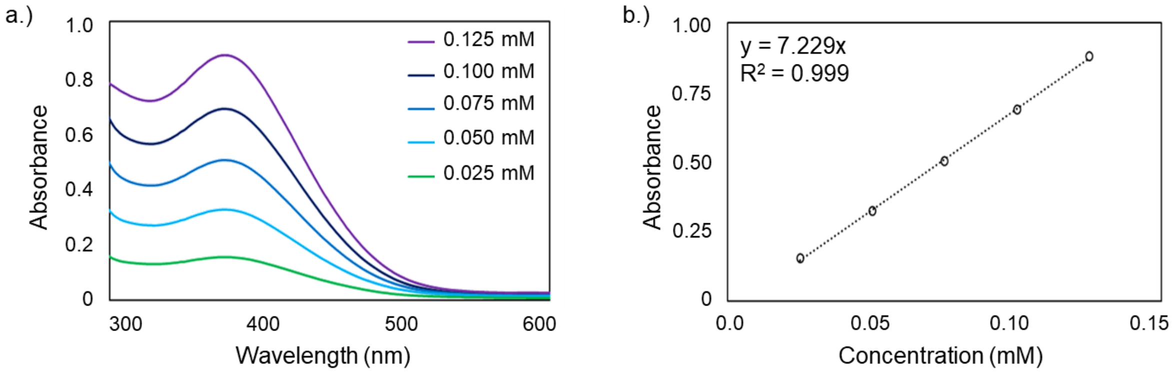

Trial	Absorbance (388 nm)	Dilute Concentration (mM)	Dilution	Saturated Concentration (M)
1	0.9327	0.129	10 µL to 30 mL	0.387
2	0.9692	0.134	10 µL to 30 mL	0.402
3	0.9819	0.136	10 µL to 30 mL	0.408

Average Concentration = 0.399 ± 0.011 M

Figure S19. Beer's Law plots and solubility calculations for **2-Pentyl** in MeCN with 0.1 M [^{n}Bu$_4$N][PF$_6$]. Absorption spectra blanked with 0.1 M [^{n}Bu$_4$N][PF$_6$].

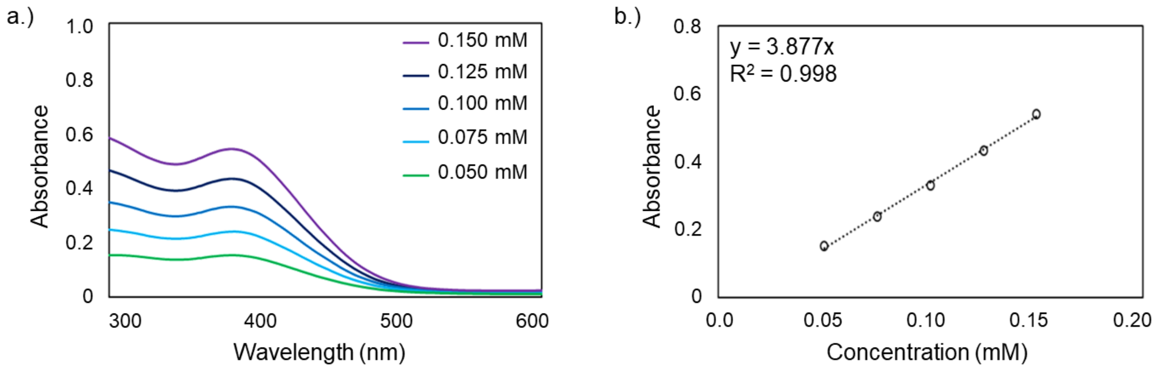

Trial	Absorbance (384 nm)	Dilute Concentration (mM)	Dilution	Saturated Concentration (M)
1	0.5195	0.134	10 µL to 20 mL	0.268
2	0.5447	0.141	10 µL to 20 mL	0.281
3	0.4904	0.127	10 µL to 20 mL	0.253

Average Concentration = 0.267 ± 0.014 M

Figure S20. Beer's Law plots and solubility calculations for **2-Hexyl** in MeCN with 0.1 M $[^{n}Bu_4N][PF_6]$. Absorption spectra blanked with 0.1 M $[^{n}Bu_4N][PF_6]$.

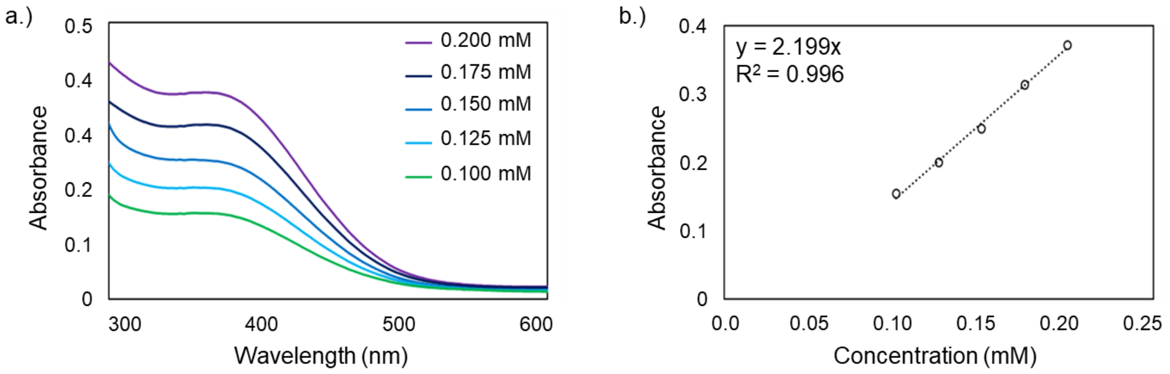

Trial	Absorbance (384 nm)	Dilute Concentration (mM)	Dilution	Saturated Concentration (M)
1	0.2749	0.125	10 µL to 10 mL	0.125
2	0.3123	0.142	10 µL to 10 mL	0.142
3	0.2793	0.127	10 µL to 10 mL	0.127

Average Concentration = 0.131 ± 0.009 M

Figure S21. Plots of ΔE_p vs. (v) and i_p vs. $\sqrt{v}$ for **1-Pentyl**

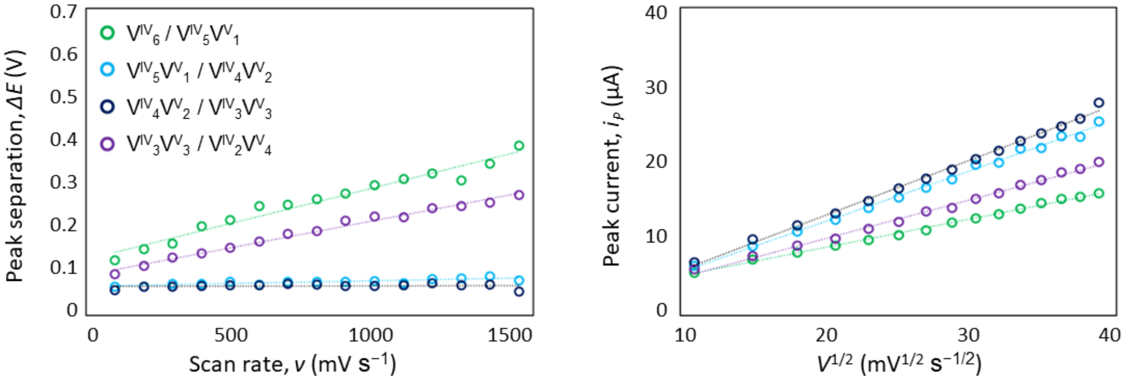

Figure S22. Plots of ΔE_p vs. (v) and i_p vs. $\sqrt{v}$ for **2-Ethyl**

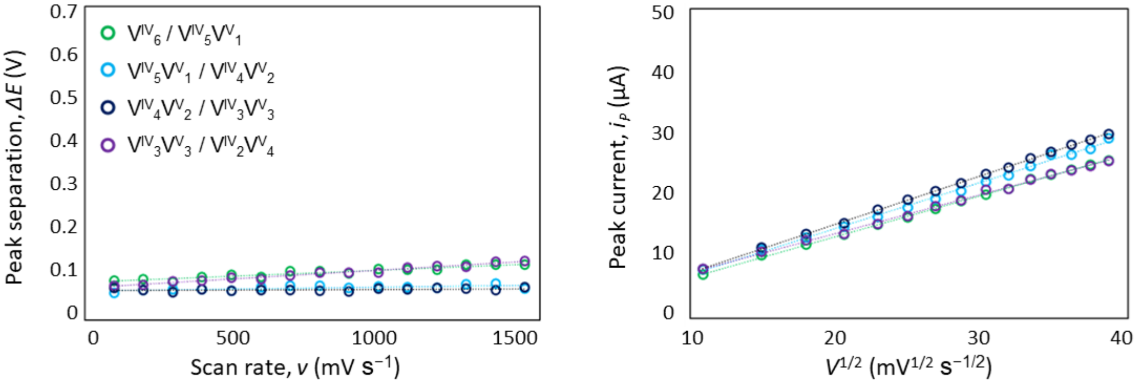

Figure S23. Plots of ΔE_p vs. (v) and i_p vs. $\sqrt{v}$ for **2-Propyl**

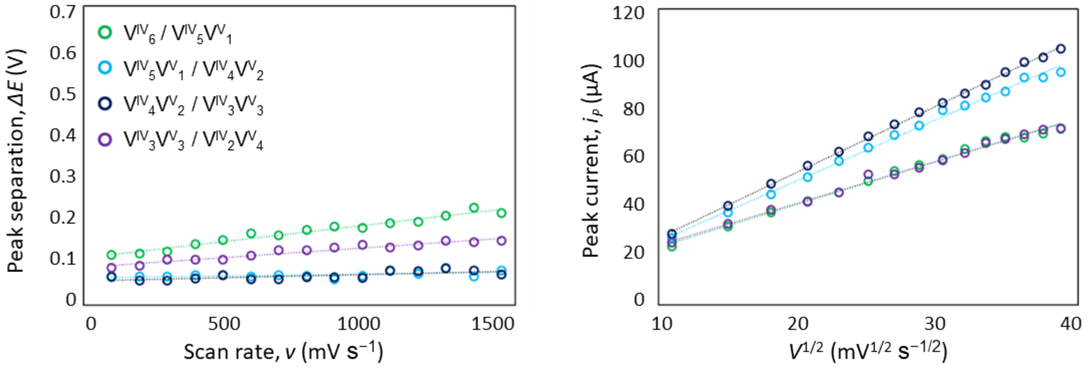

Figure S24. Plots of ΔE_p vs. (v) and i_p vs. $\sqrt{v}$ for **2-Butyl**

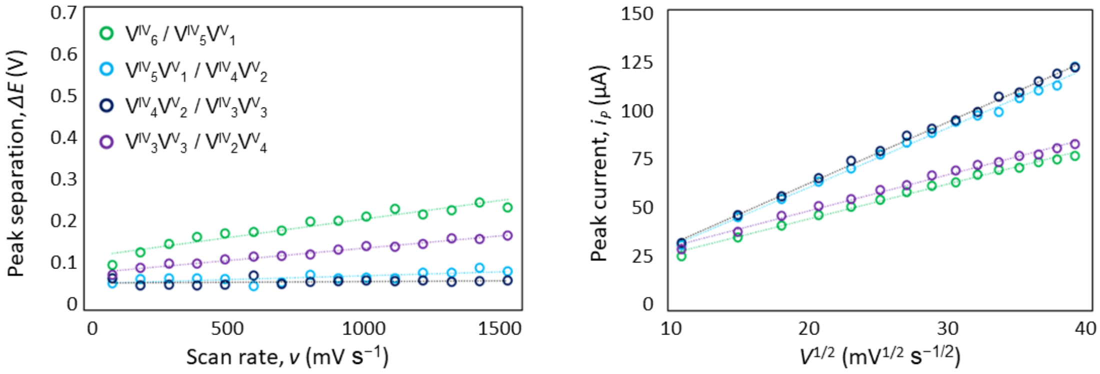

Figure S25. Plots of ΔE_p vs. (v) and i_p vs. $\sqrt{v}$ for **2-Pentyl**

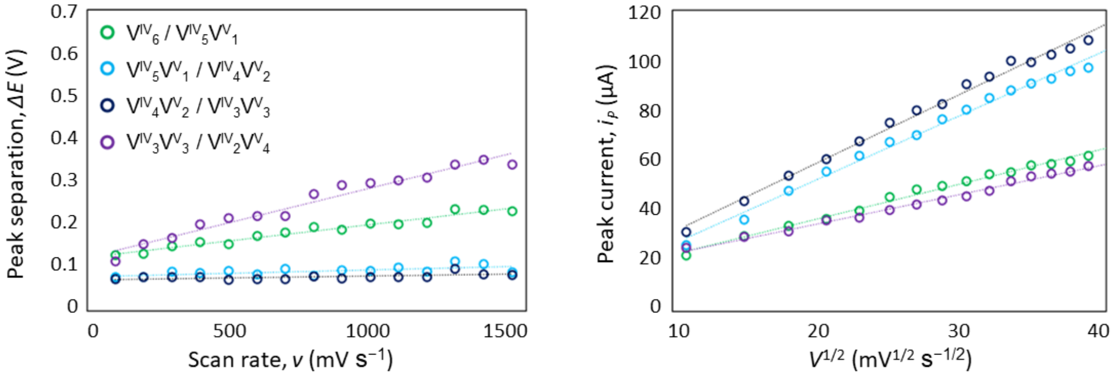

Figure S26. Plots of ΔE_p vs. (v) and i_p vs. $\sqrt{v}$ for **2-Hexyl**

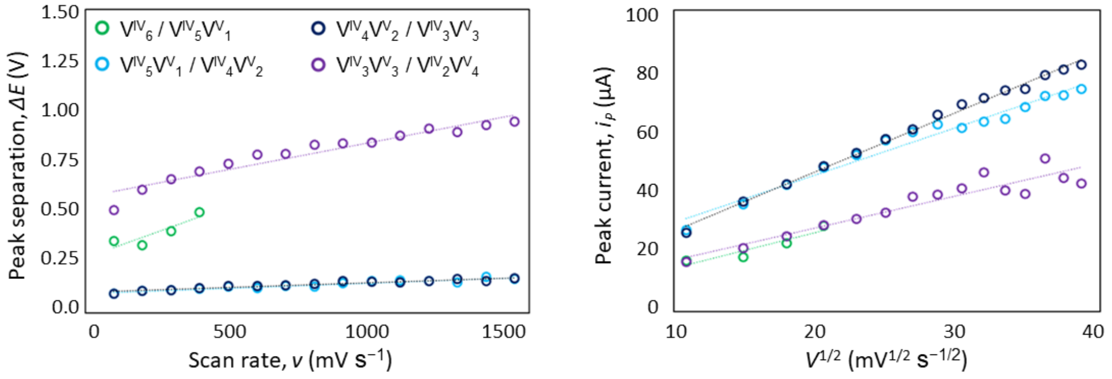

Figure S27. CV of **1-Hexyl** (1 mM) in MeCN with 0.1 M [^{n}Bu$_4$N][PF$_6$] recorded at 500 mV/s. We attribute the lack of current response at higher scan rates to the relatively slow diffusion of this molecule.

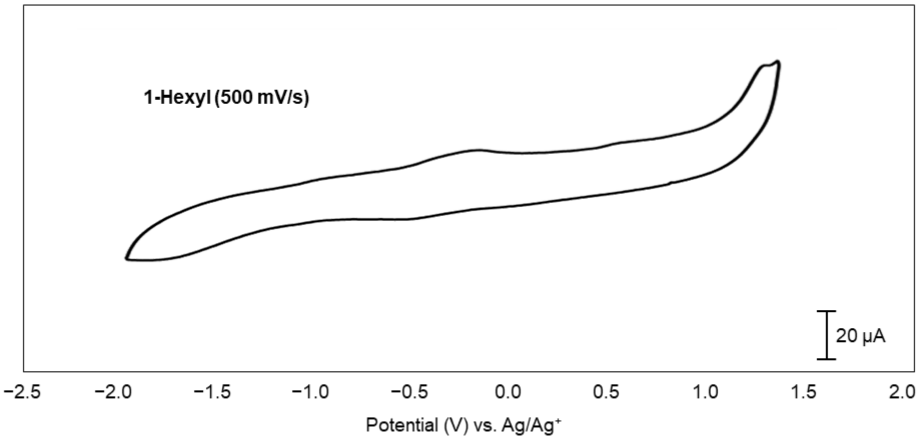

Figure S28. CV of **1-Pentyl** before and after bulk oxidation and bulk reduction of solutions. Arrows indicate open circuit potential and sweep direction.

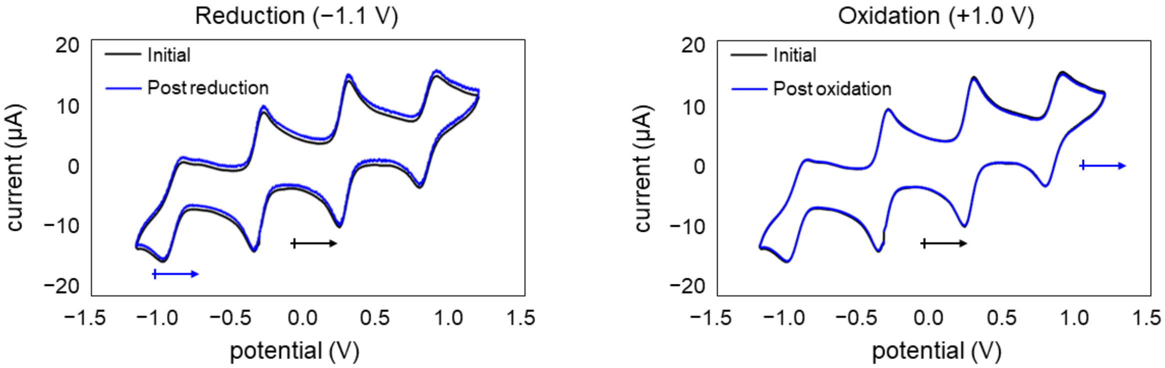

Figure S29. CV of **2-Ethyl** before and after bulk oxidation and bulk reduction of solutions. Arrows indicate open circuit potential and sweep direction.

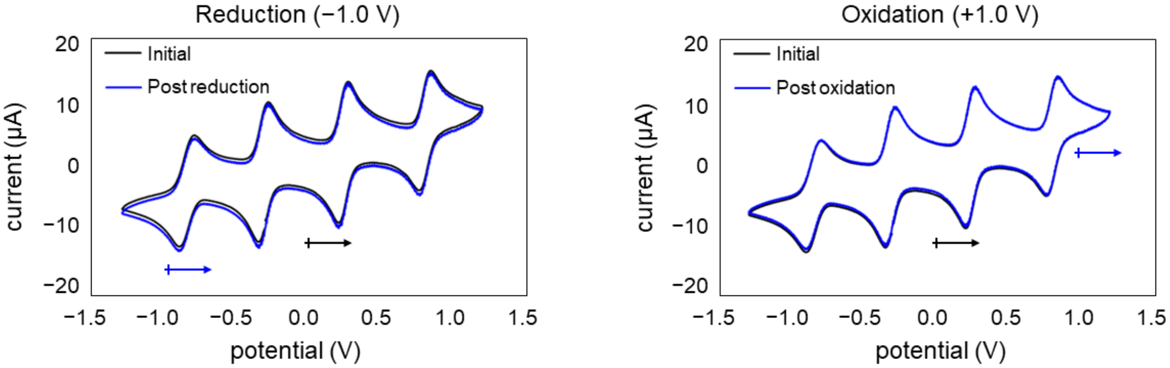

Figure S30. CV of **2-Propyl** before and after bulk oxidation and bulk reduction of solutions. Arrows indicate open circuit potential and sweep direction.

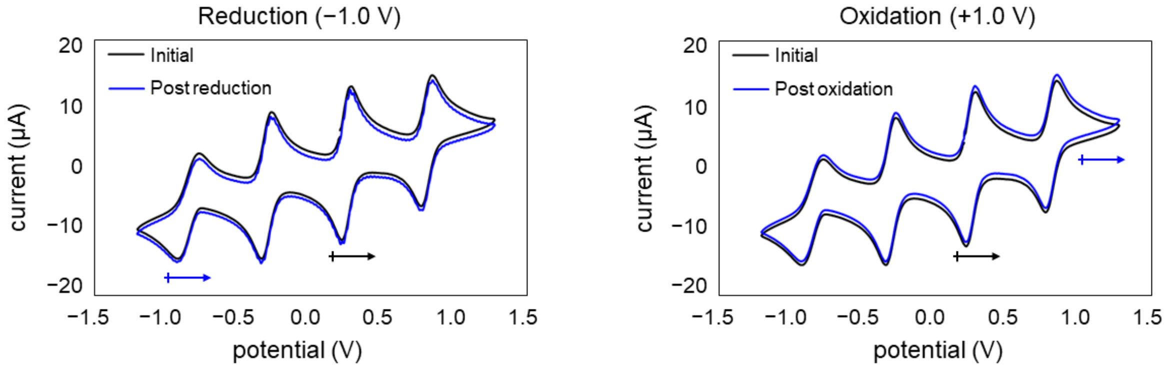

Figure S31. CV of **2-Butyl** before and after bulk oxidation and bulk reduction of solutions. Arrows indicate open circuit potential and sweep direction.

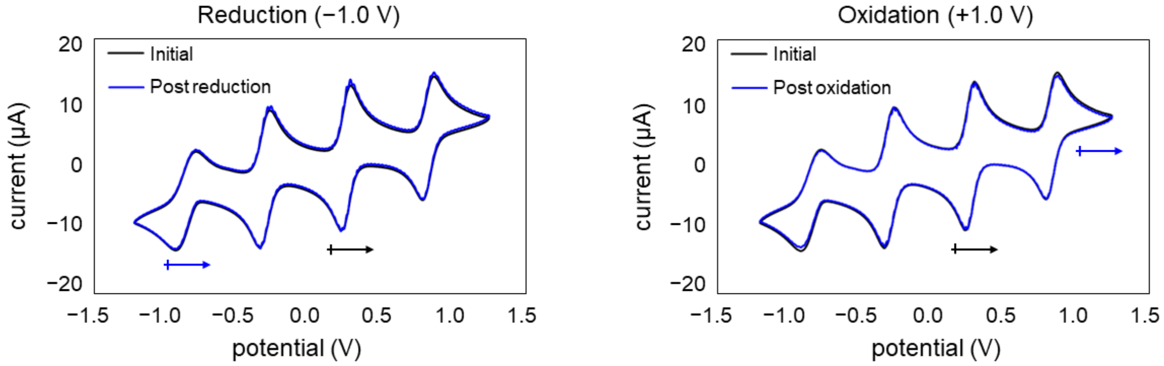

Figure S32. CV of **2-Pentyl** before and after bulk oxidation and bulk reduction of solutions. Arrows indicate open circuit potential and sweep direction.

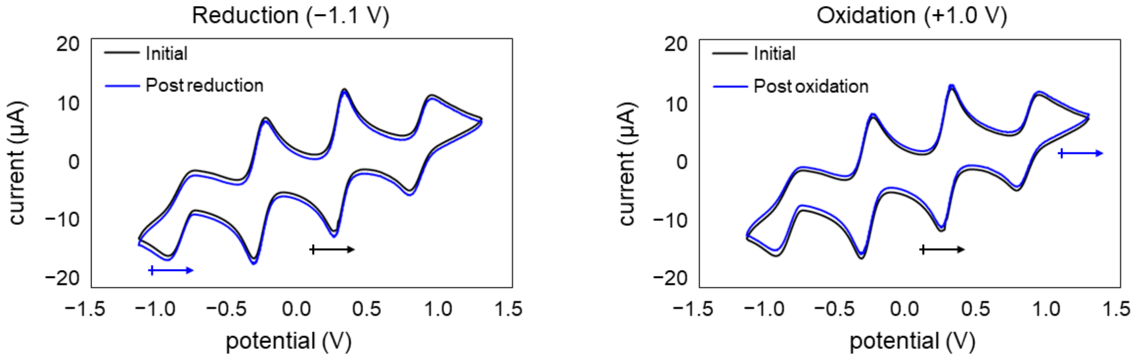

Figure S33. CV of **1-Hexyl** before and after bulk oxidation and bulk reduction of solutions. Arrows indicate open circuit potential and sweep direction.

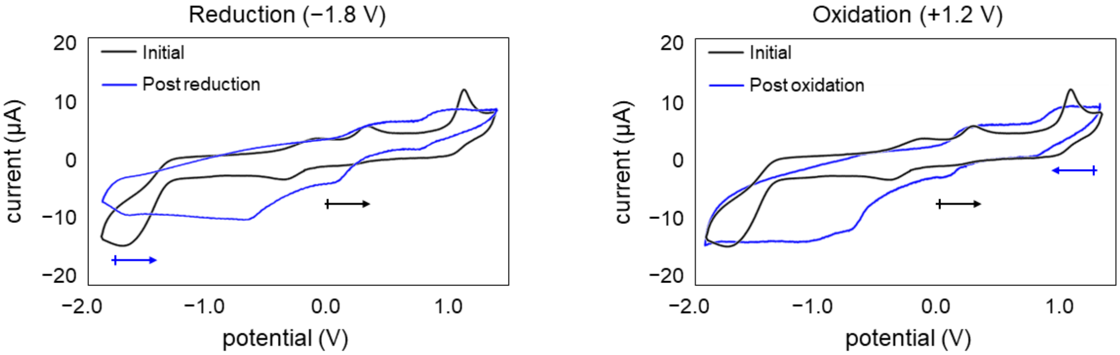

Figure S34. CV of **2-Hexyl** before and after bulk oxidation and bulk reduction of solutions. Arrows indicate open circuit potential and sweep direction.

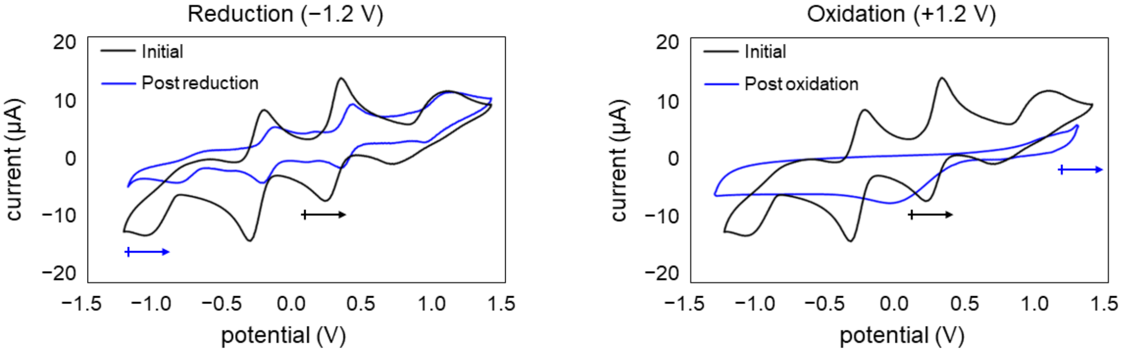

Figure S35. Charge-discharge experiments with (a) **1-Propyl** and (b) **2-Propyl**. Experiments were conducted in an H-cell with identical solutions in each half-cell (2mM cluster, 0.1 M $[NBu_4][PF_6]$, 5 mL MeCN. Galvanostatic cycling at 0.4 mA, with potential cut-offs of 2.0 V charging and 0.1 V discharging. Voltage trace of cycles 2-7. CV before and after charging evidence the stability of both charge carriers.

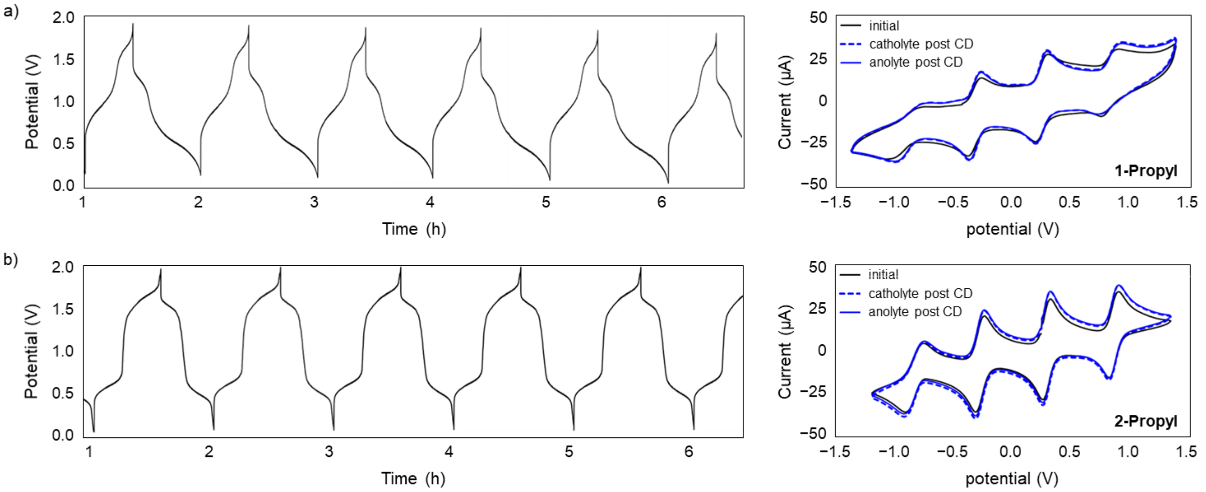

Figure S36. Charge-discharge experiments with (a) **1-Butyl** and (b) **2-Butyl**. Experiments were conducted in an H-cell with identical solutions in each half-cell (2mM cluster, 0.1 M $[NBu_4][PF_6]$, 5 mL MeCN. Galvanostatic cycling at 0.4 mA, with potential cut-offs of 2.0 V charging and 0.1 V discharging. Voltage trace of cycles 2-7. CV before and after charging evidence the stability of both charge carriers.

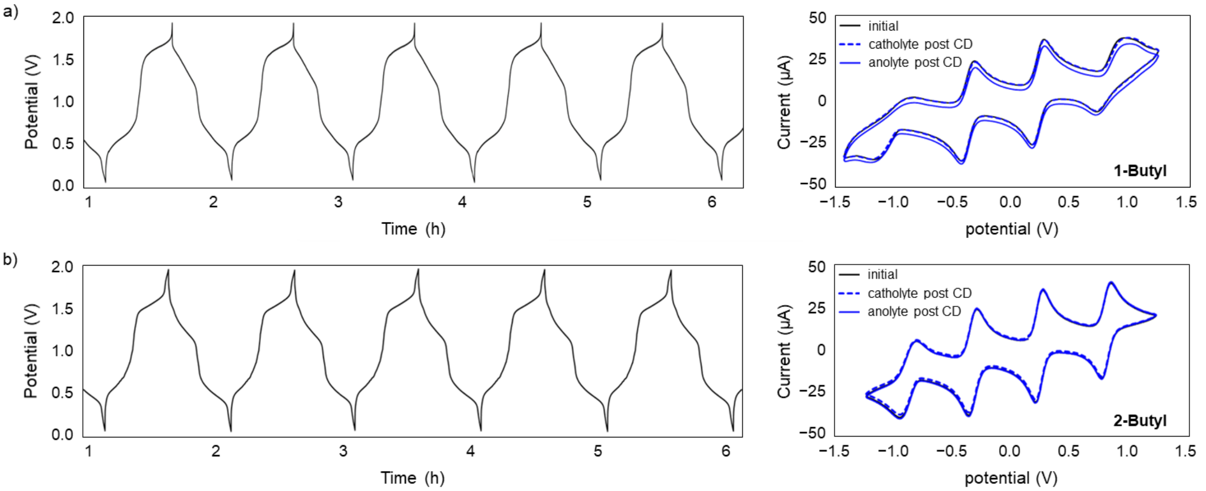

Figure S37. Plots of coulombic efficiency for each cycle in charge discharge experiments with (a) **1-Pentyl** and (b) **2-Pentyl**. No difference in coulombic efficiency is observed.

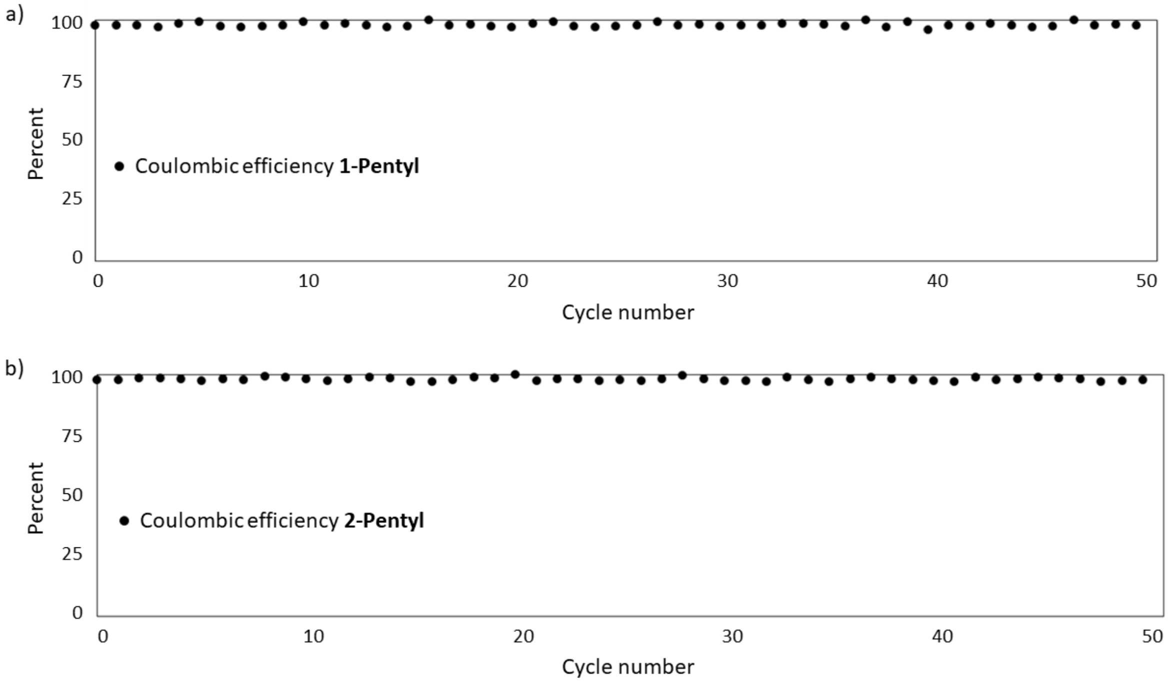

References.

1. C. Daniel and H. Hartl, *Journal of the American Chemical Society*, 2005, **127**, 13978-13987.
2. A. M. Kosswattaarachchi, L. E. VanGelder, O. Nachtigall, J. P. Hazelnis, W. W. Brennessel, E. M. Matson and T. R. Cook, *J. Electrochem. Soc.*, **2019,** *166,* A1-A9. DOI: 10.1149/2.1351902jes
3. Q. Liu, A. E. S. Sleightholme, A. A. Shinkle, Y. Li and L. T. Thompson, *Electrochemistry Communications*, 2009, **11**, 2312-2315.
4. A. E. S. Sleightholme, A. A. Shinkle, Q. Liu, Y. Li, C. W. Monroe and L. T. Thompson, *Journal of Power Sources*, 2011, **196**, 5742-5745.
5. A. M. Kosswattaarachchi, A. E. Friedman and T. R. Cook, *ChemSusChem*, 2016, **9**, 3317-3323.
6. R. S. Nicholson and I. Shain, *Analytical Chemistry*, 1964, **36**, 706-723.
7. H. Muhammad, I. A. Tahiri, M. Muhammad, Z. Masood, M. A. Versiani, O. Khaliq, M. Latif and M. Hanif, *Journal of Electroanalytical Chemistry*, 2016, **775**, 157-162.